SUPPORTING INFORMATION

Nanoparticle-based superchain networks formed by the side-by-side self-assembly of soft magnetite nanorods

Madeleine Alexandra Schaefer,[a] Sebastian Polarz[a] and Irene Morales[a,b,*]

[a] Institute of Inorganic Chemistry, Leibniz University Hannover, Callinstrasse 9, 30167, Hannover, Germany

[b]Cluster of Excellence PhoenixD (Photonics, Optics and Engineering- Innovation Across Disciplines), Leibniz University Hannover, 30167 Hannover, Germany

Table of Contents

Supplementary Figures

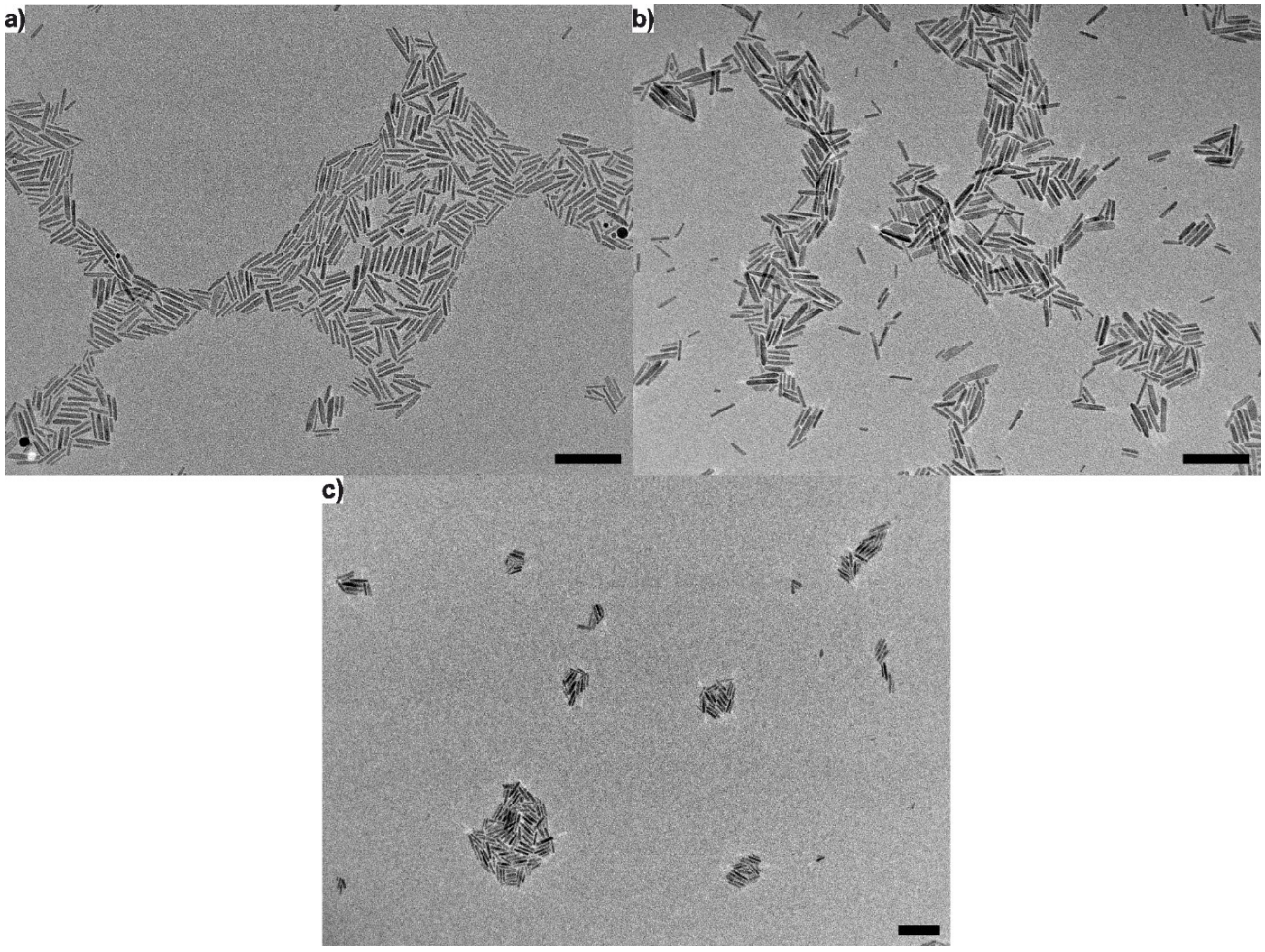

Figure S1. TEM images of nanorods obtained using a) Octylamine b) dodecylamine and c) oleyl amine as ligand (scale bars = 100 nm).

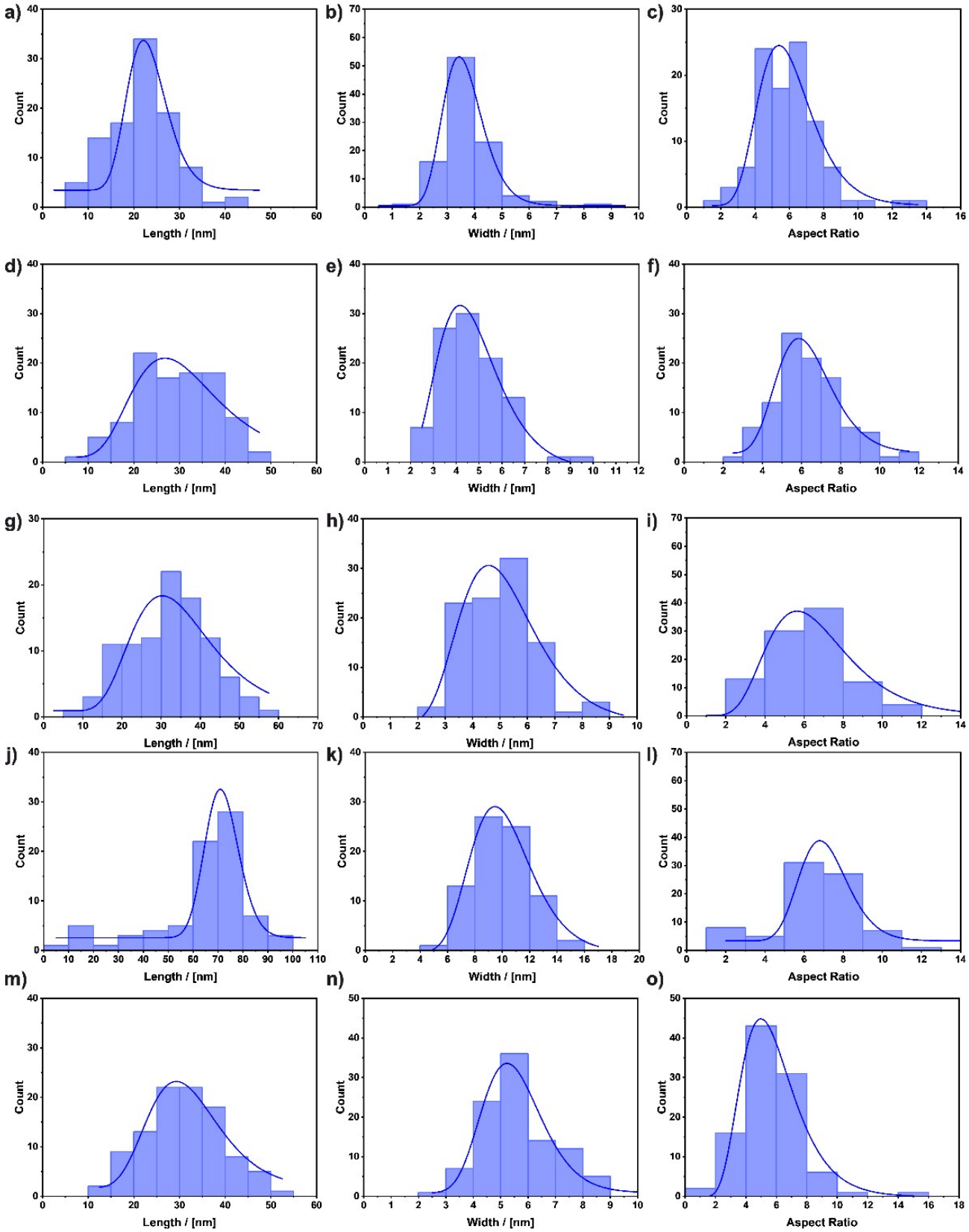

Figure S2. Lognormal distribution of a-c) propylamine, d-f) octylamine, g-i)dodecylamine, j-l) hexadecylamine, m-o) oleylamine-capped nanorods. a,d,g,j,m) show the length of the nanorods, b,e,h,k,n) the width and c,f,i,l,o) the calculated aspect ratios of the particles. 100 particles were measured in length and width and the aspect ratio was calculated for each particle individually.

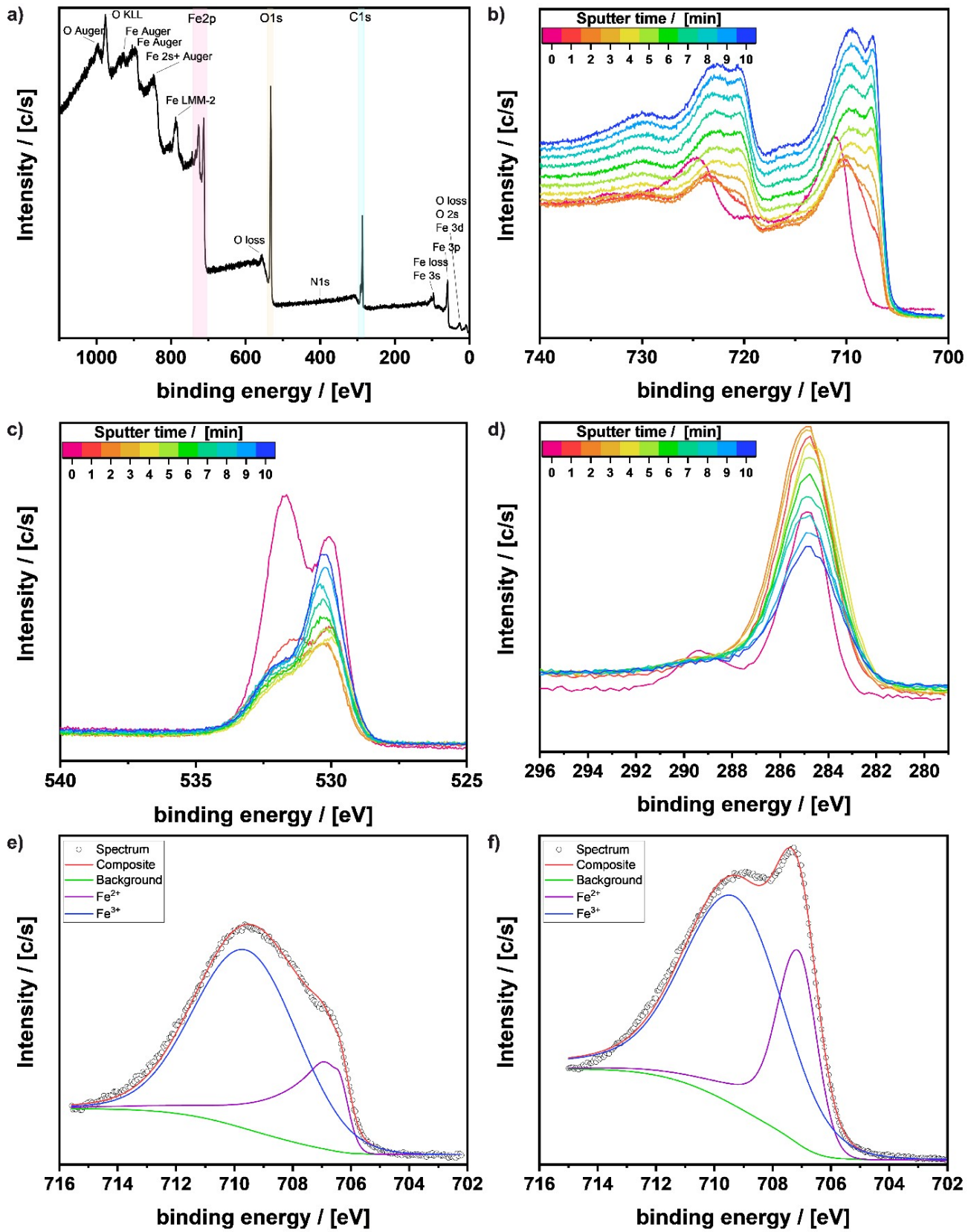

Figure S3. XPS data of dried powdered nanorods. a) Sweep of the surface with labeled peaks and b-d) profile data of b) Fe2p, c) O1s and d) C1s obtained by sputtering with argon (2kV) for one minute each for 10 minutes total. The colors transition from pink (surface, 0 min) to blue (10 min) as indicated by the legend. e,f) The Fe^{2+} and Fe^{3+} peaks were fitted after sputtering for e) 1 min and f) 10 min.

The spectra are shifted to the C1s peak as standard procedure. The resulting shift in peak appearance in the Fe2p and O1s spectra is likely caused due to the higher amount of surface in the first measurements. Sputtering the material longer removes the first surface layers and thus leads to a material which consist of both the bulk magnetite in the nanoparticle cores and the surface layers between nanorods.

In the surface only Fe^{3+} is present, which indicates the presence of maghemite or hematite. This is clearly visible by the shift in binding energy and peak shape observed through sputtering as this removes part of the particle surfaces. Calculating the amount of Fe^{3+} from the observed binding energies results in 75.6% Fe^{3+} after one minute of sputtering and 71.2% after 10 minutes. As the ideal stoichiometry of magnetite would be 66.7% Fe^{3+} and the surface of the particle sample is only showing Fe^{3+}, this indicates that the inside of the particles consists of magnetite, while the surfaces between the particles can be attributed to the slight over presence of Fe^{3+}. Similar observations have been reported of citrate-coated magnetic nanoparticles.[1]

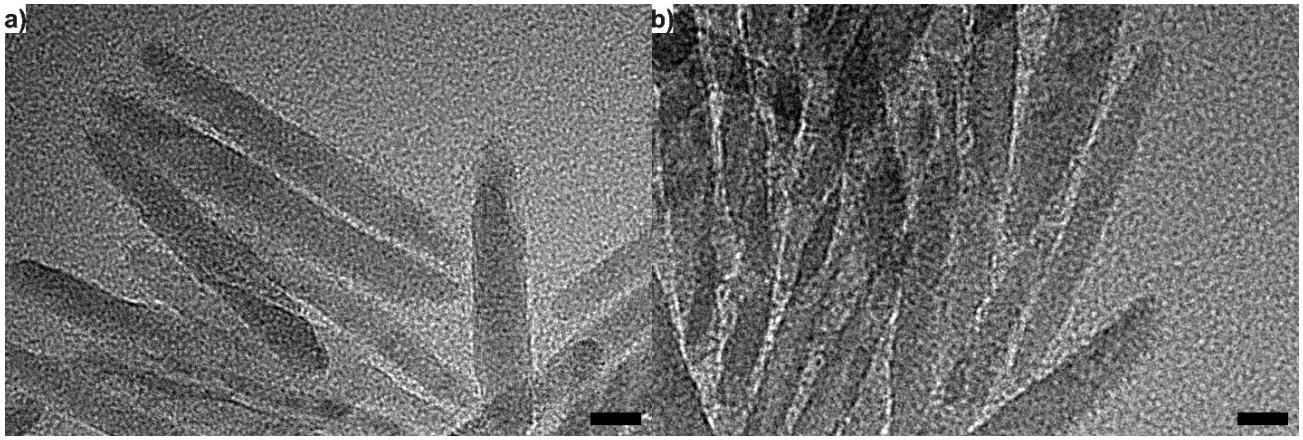

Figure S4. HR-TEM images of multiple magnetite nanorods showcasing the lattice planes and thus monocrystalline quality of the samples (scale bar = 10 nm).

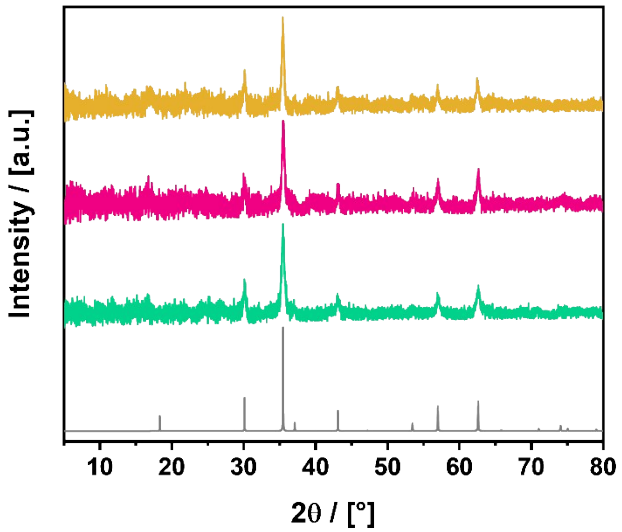

Figure S5. XRD data of octylamine (green), dodecylamine (magenta) and oleylamine (yellow) capped nanorods compared to calculated intensities of magnetite using Vesta[2] (grey, cif151330128[3]).

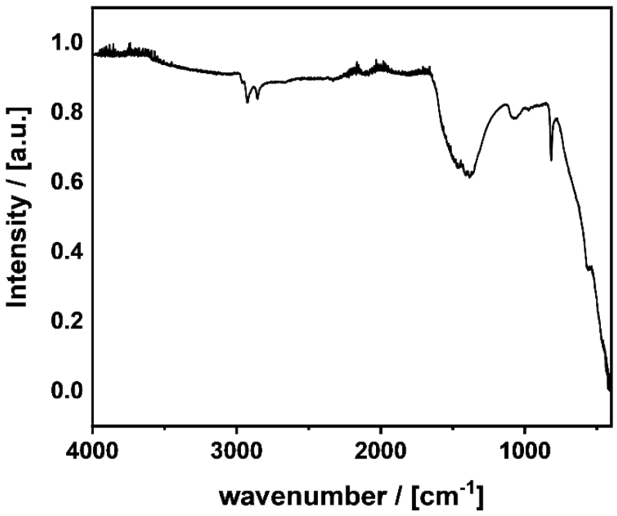

Figure S6. Normalized IR Data spectrum of obtained 70 nm nanorods. Assigned bands are listed in Table S1.

Table S1. Assigned IR data.

Vibration [cm^{-1}]	**Assigned Bond**
3576	-O-H
2918	$-CH_2-$
2850	$-C-H_3$
1705	-COOH
1453	$-COO^-$
1376	$-COO^-$
1061	-C-O-
965	-HC=CH-
809	$R-NH_2$
549	Fe-O
< 400	Fe-O

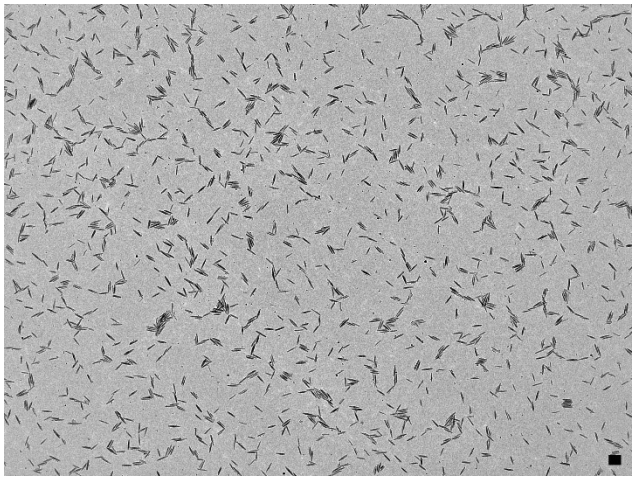

Figure S7. TEM micrographs of 70MagNR at low particle density; scalebar = 100 nm.

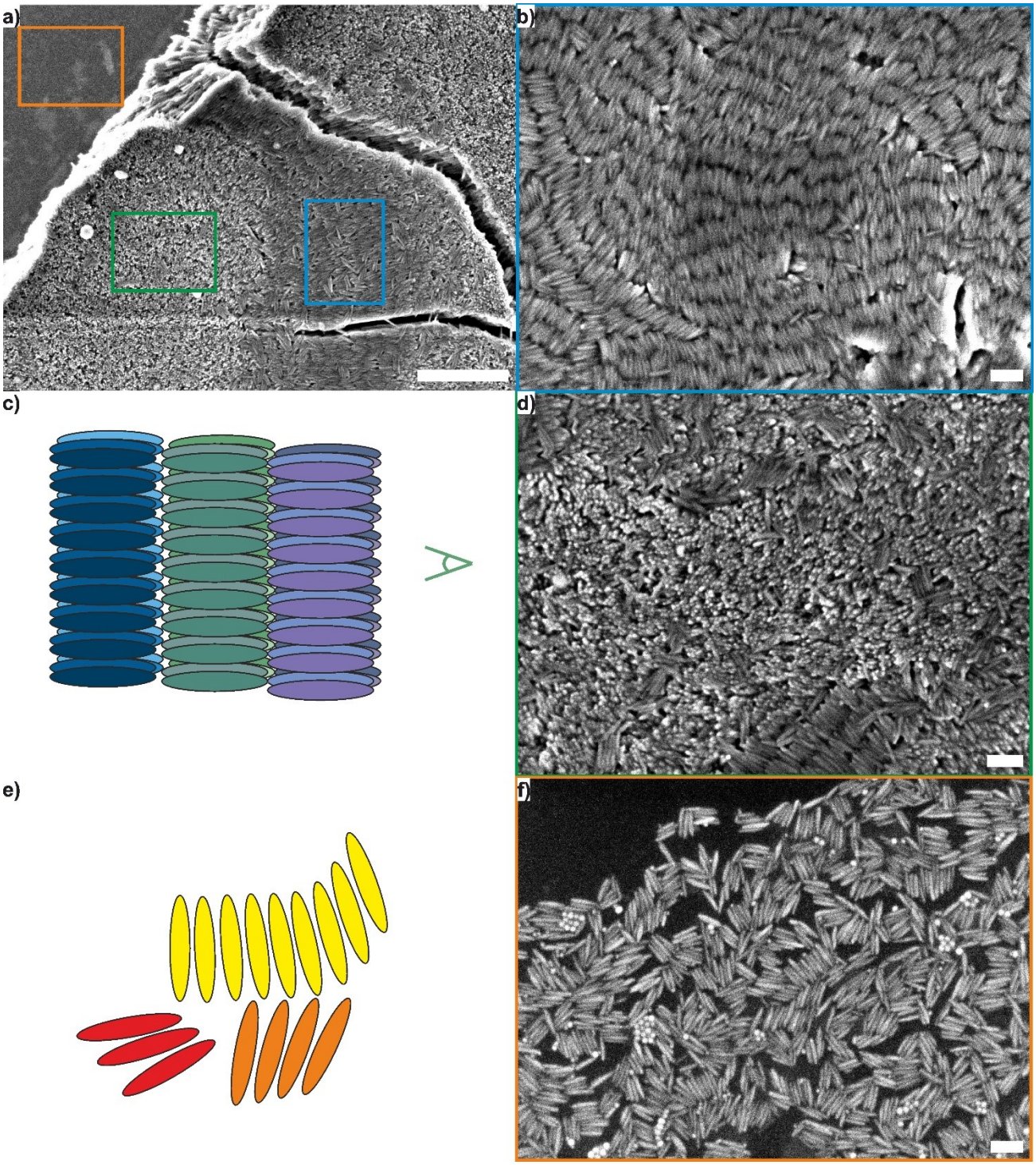

Figure S8. SEM images of an overview an assembled sample of 70 nm nanorods with a visible drying crack showcasing the rotation of the nanorods in the superstructure (a, scale bar = 500 nm) and individual areas representing: chain like alignment in-plane (b, scale bar = 100 nm) and out of plane (d, scale bar = 100 nm) with high local particle density and monolayer areas with bundle formation (f, scale bar = 100 nm) in low denisity areas. c) Sketch of the superchain arrangement as viewed in b) and viewpoint of d) indicated in green. The nanorods align longitudinal in a certain width and tip-to-tip with nanorods in the neighboring chain forming 3D structures. e) sketch of structural motifs in monolayers showing bundle to small chain arrangements, in which only few nanorods align with each other in side-by-side structures.

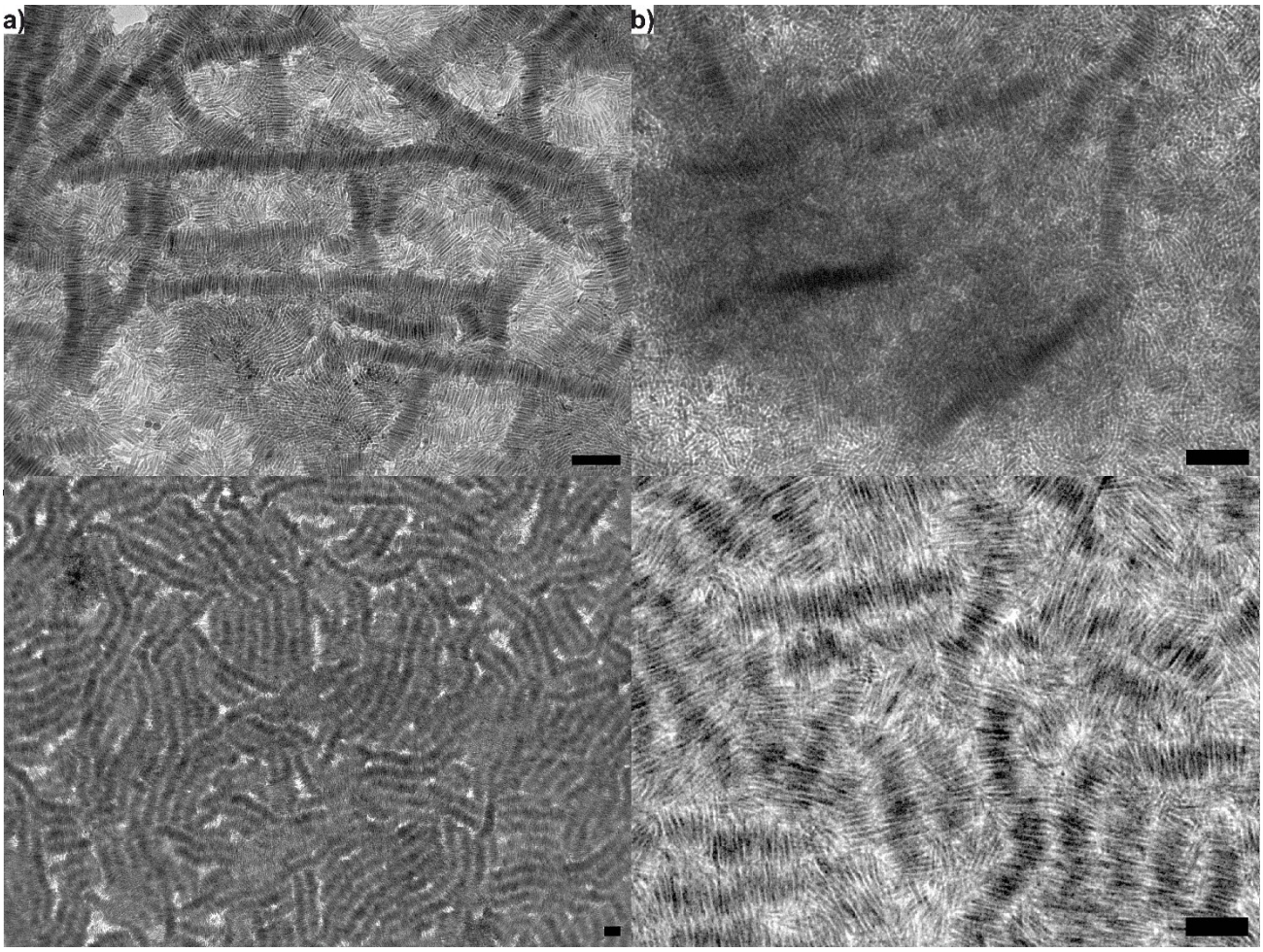

Figure S9. Reproduction of the assembly protocols for a,b) 30MagNR and c,d) 70 MagNR. Images a, c) show the nanoparticle batch discussed in the paper, while b, d) show an independent assembly with another nanoparticle batch to prove the reproducibility of the structures (scale bars = 100 nm).

Table S2. Coercivity (H_C) and saturation magnetization (M_S) of the obtained nanorods at 5 K and 300 K obtained from the hysteresis shown in **Fig. 6a**.

Nanorod Size	H_C at 5 K [Oe]	H_C at 300 K [Oe]	M_S at 5 K [emu g-1]	M_S at 300 K [emu g-1]
30 nm	266.17	16.31	62.91	57.21
70 nm	145.87	9.21	68.27	62.61

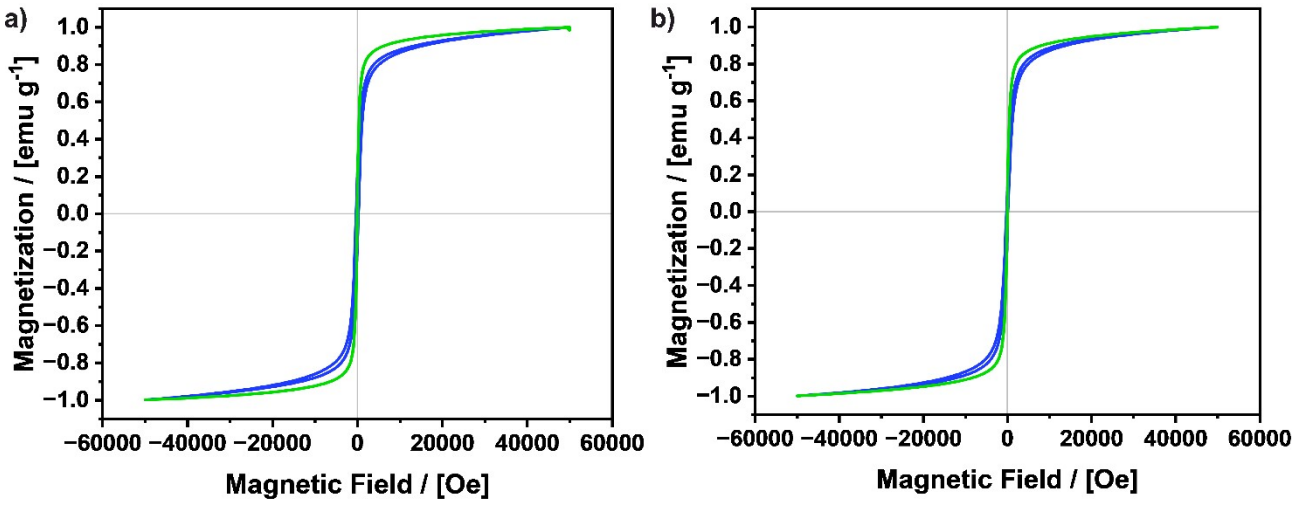

Figure S10. Normalized SQUID hysteresis measurements of a) dried nanorods dispersed in cotton and measured in DC mode in a gelatin capsule and b) dried powder measured in VSM mode at 5 K (blue) and 300 K (green) each. The obtained spectra showcase the same significant features, therefore confirming that the powder sample preparation for SQUID does not lead to a preferential orientation within the sample holder.

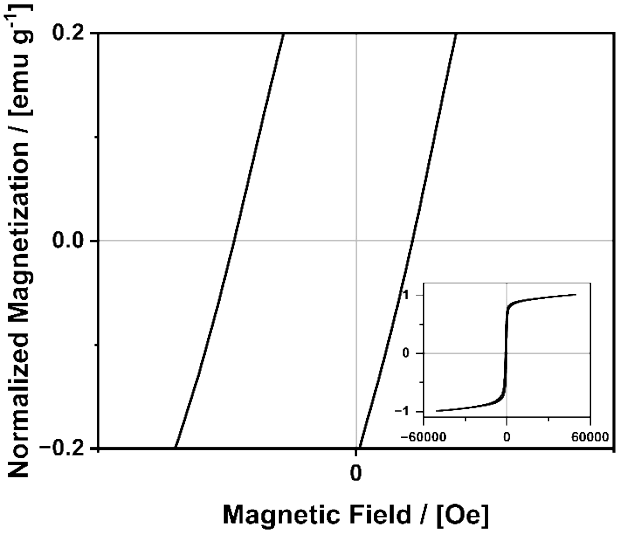

Figure S11. Normalized SQUID hysteresis measurements of 70MagNRs obtained at 5 K after field-cooling at 2 T, showcasing exchange bias. This observation, along with the wasp-like features present in **Fig. 6a**, confirms that both phases are not independent, but in an interacting core-shell configuration.

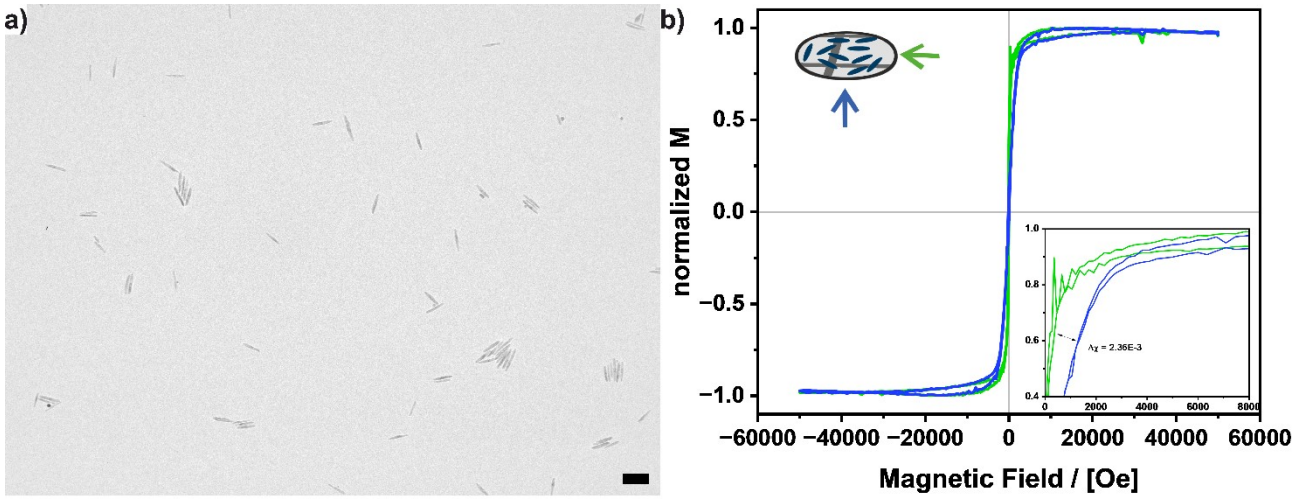

Figure S12. a) Dropcasted nanorods laying scattered around the substrate in plane (scale bar = 100 nm). b) Normalized magnetization of drop casted nanorods on an Si substrate measured in (green) and out of plane (blue) direction, corrected for the diamagnetic response (**Supplementary Information B**).

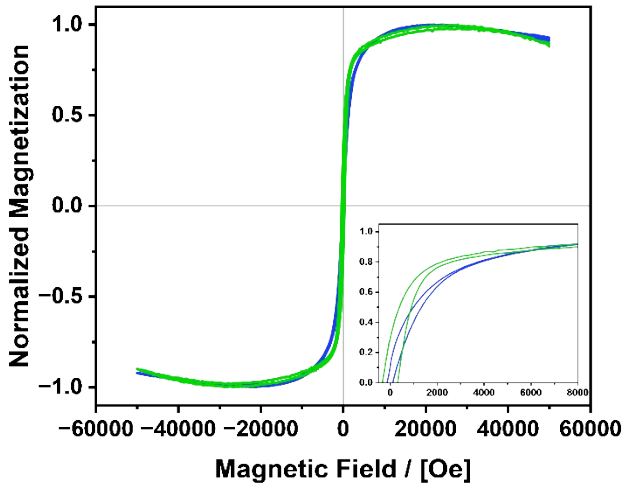

Figure S13. Assembled nanorods measured in plane (green) and out of plane (blue) at 5 K.

Table S3. Susceptibilities of 70 nm nanorods compared for dropcasted, assembled and random oriented nanorods in out-of-plane and in-plane directions. The values were obtained by linear regression in the range of ±200 Oe of the hysteresis cycle.

Sample	$\chi_{in\text{-}plane}$ [Oe^{-1}]	$\chi_{out\text{-}of\text{-}plane}$ [Oe^{-1}]	$\Delta\chi$ [Oe^{-1}]
Dropcasted Nanorods (**Figure S17b**)	3.07E-03 ± 2.03E-05	7.05E-04 ± 4.87E-05	2.36E-03
Assembled Nanorods (**Figure 6c**)	2.74E-03 ± 8.22E-05	1.06E-03 ± 1.20E-05	1.68E-03
Random oriented nanorods (**Figure S16**)	1.72E-03 ± 3.20E-05		-

Measurement Details

Supplementary Information A. ICP-OES

ICP-OES samples were prepared as described in the experimental details and diluted to gain samples which were approximated to be within the calibrated values using TG measurement values. A linear calibration was set-up using diluted stock solution (ROTI©Star 10 000 mg/l Fe, Carl Roth) at 1 mg L^{-1}, 3 mg L^{-1}, 5 mg L^{-1}, 7.5 mg L^{-1} and 10 mg L^{-1}. Multiple emission lines of Fe were then calibrated as shown in **Figure S11** and **Table S4** shows the obtained correlation coefficients. The obtained concentrations that were calculated by ICP Expert II, the standard deviation and an average concentration and the deviation of the different emission lines are calculated and shown in **Table S5**. To calculate the organic content, the sample was assumed to be pure magnetite and the atomic masses were used to calculate the total percentage of iron oxide. The resulting mass differences between the mass used for the measurement and the calculated mass of magnetite is then equal to the organic content of the sample (**Eqn. (1)**).

$$organic\ content\ = \left[m(sample) - \ m(ICP - OES) \cdot \frac{168}{232}\right] \cdot 100\ wt\% \quad (1)$$

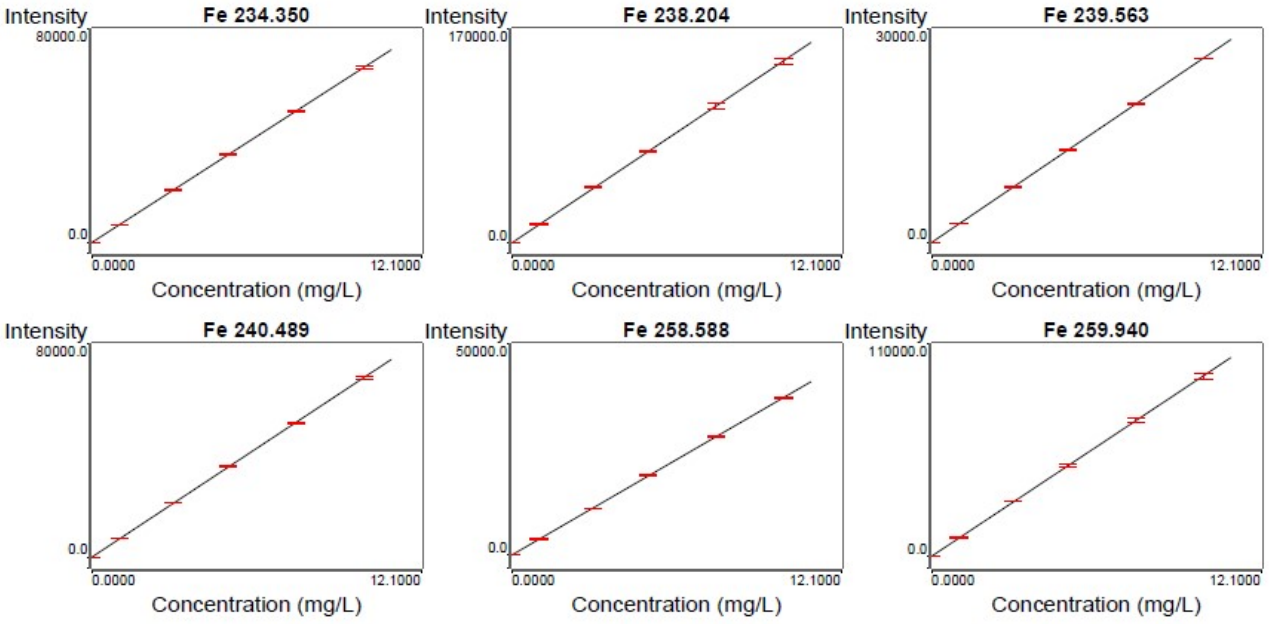

Figure S14. Calibration data of the ICP-OES.

Table S4. Used emission lines with correlation coefficient.

Emission line	Correlation Coefficient
234.350	0.999994
238.204	0.999980
239.563	0.999974
240.489	0.999964
258.588	0.999966
259.940	0.999965

Table S5. Obtained concentrations and standard deviation for each emission line and averaged for all samples.

Used Amine	Averaged c Fe [%]	Averaged c Fe_3O_4 [%]	Organic content [%]
HDA	57.37	79.23	20.77
DoAm	60.43	83.44	16.55
OcAm	60.55	83.62	16.38
PrAm	62.73	86.63	13.37

Supplementary Information B. SQUID

SQUID data was recorded in VSM mode using powder (brass) or substrate sample holders (brass or quartz) as appropriate. Powdered samples were normalized for their iron content obtained as detailed in **Supplementary Information A**.

In the case of nanoparticles on a Si substrate, we subtracted the diamagnetic response of both substrate and sample holder. This correction was performed by fitting the linear high-field behavior of the magnetization curve, where the ferrimagnetic sample had already reached saturation. In this high-field region, the observed linear trend was attributed to the diamagnetic components, allowing us to perform a linear fit that was removed from the total signal. In the case of the assembled nanorods shown in **Figure 6d**, the signals were initially corrected by measuring and subtracting the background signal from an empty Cu grid, using the same sequence as for the sample. The signals were additionally corrected for the diamagnetic response of the Kapton tape used to attach the samples as detailed above. The curves were then normalized to allow easy comparison between them.

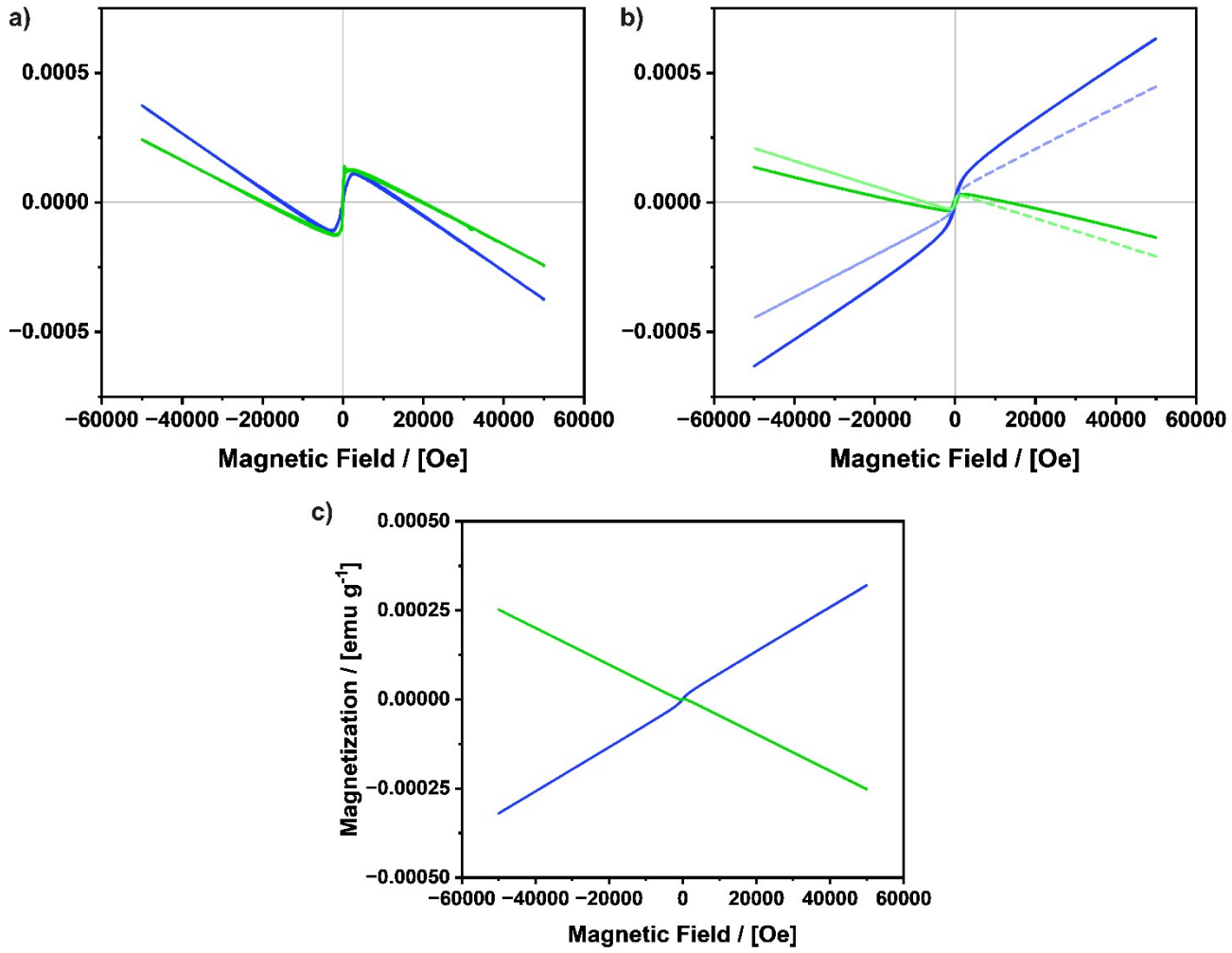

Figure S15. Raw data of Figure 6c and Supplementary Figure 17. a) Not corrected in plane (green) and out of plane (blue) magnetization of dropcasted nanorods on a silicon wafer at 300 K. b) not corrected in plane (green) and out of plane (blue) magnetization of superchains assembled on a Cu TEM grid at 5 K (continuous line) and 300 K (segmented line). c) signals of the Cu-TEM grid in plane (green) and out of plane (blue) at 300 K used to correct the data presented in b).

Supplementary Information C: Calculations of Magnetic Dipole-Dipole Interactions

To characterize the strength of the magnetic dipole-dipole interaction based on the magnetic coupling parameter *Γ*, first the volume of the individual rod V_{NR} was calculated assuming a perfect cylinder as idealized shape of our nanorods and using the width w_{NR} and length l_{NR} of the nanorod. For this, the statistically evaluated values from **Table 1** were used, resulting in:

$$V_{NR} = \pi r^2 h = \pi \cdot \left(\frac{w_{NR}}{2}\right)^2 \cdot l_{NR} \quad (2)$$

The center-to-center distance *d* can be calculated by using the width of the nanorod w_{NR} and the observed distance between nanorods, which corresponds to the size of the organic ligand l_L on the surface:

$$d = w_{NR} + l_L \quad (3)$$

Using the measured saturation value M_S as listed in **Table S2** from the 300K MH hysteresis measurements, the previously obtained volume of the ideal nanorod and the density of magnetite ρ = 5.18 g cm^{-3},[4] we can calculate the individual magnetic saturation of each nanorod m_S:

$$m_S = M_S * V_{NR} * \rho \quad (4)$$

Using the well-established **formula (4)**[5,6], the magnetic coupling parameter *Γ*, can be calculated using the above-mentioned parameters and the magnetic constant μ_0, the Boltzmann constant k_B and the temperature T. For the derivation of the formula, we would like to refer the reader to literature.[5,6] To summarize the meaning of the constant, *Γ* is the factor resulting of the maximum attractive dipole-dipole interaction energy U_{DD} divided by the thermal energy U_{Th} of the system. Hence, for values of *Γ >> 1,* the magnetic interactions are larger than the thermal agitation of the system.

$$\Gamma = \frac{U_{DD}}{U_{Th}} = \frac{\mu_0 m_S^2}{2\pi d^3 k_B T} \quad (5)$$

Additionally, we calculated the magnetic Bjerrum length λ_B, which describes the distance in which the magnetic interactions are significant compared to the thermal interactions for our particle system[5,6]. This means that the shorter nanorods need to be closer to interact magnetically, than the larger nanorods.

$$\lambda_B = \left[\frac{\mu_0 m_s^2}{2\pi k_B T}\right]^{\frac{1}{3}} \quad (6)$$

Table S6. Calculated parameters for 70magNR and 30magNR.

Nanorod Size	***Γ***	**λ_B / [nm]**
30 nm	7.79	13.19
70 nm	114.84	54.39

Notes and references

Abbreviations

AR; aspect ratio; DLS, dynamic light scattering; HR-TEM, high resolution transmission electron microscopy; ICP-OES, inductively coupled plasma optical emission spectroscopy; IR, infrared spectroscopy; SEM, scanning electron microscopy; SQUID, superconducting quantum interference device; TEM, transmission electron microscopy; XPS, X-ray photoelectron spectroscopy; XRD, X-ray diffraction; ZFCFC, zero field cooled - field cooled.

References

1 A. Atrei, B. Lesiak-Orlowska and J. Tóth, *Applied Surface Science*, 2022, **602**, 154366.
2 K. Momma and F. Izumi, *J Appl Cryst*, 2011, **44**, 1272–1276.
3 F. F. Ferreira, E. Granado, W. J. Carvalho, S. W. Kycia, D. Bruno and R. J. Droppa, *J Synchrotron Rad*, 2006, **13**, 46–53.
4 G. S. Parkinson, *Surface Science Reports*, 2016, **71**, 272–365.
5 J. Faraudo, J. S. Andreu and J. Camacho, *Soft Matter*, 2013, **9**, 6654–6664.
6 J. S. Andreu, J. Camacho and J. Faraudo, *Soft Matter*, 2011, **7**, 2336–2339.